

High-Speed Atomic Force Microscopy Reveals Loss of Nuclear Pore Resilience as a Dying Code in Colorectal Cancer Cells

Mahmoud Shaaban Mohamed^{†‡§}, *Akiko Kobayashi*^{†§}, *Azuma Taoka*^{‡§}, *Takahiro Watanabe-Nakayama*[‡], *Yosuke Kikuchi*[§], *Masaharu Hazawa*^{†§}, *Toshinari Minamoto*^{//}, *Yoshihiro Fukumori*[§], *Noriyuki Kodera*[‡], *Takayuki Uchihashi*[‡], *Toshio Ando*[‡] and *Richard W. Wong*^{†‡§*}.

[†] Cell-Bionomics Research Unit, Innovative Integrated Bio-Research Core, Institute for Frontier Science Initiative, Kanazawa University, Kakuma-machi, Kanazawa 920-1192, Japan;

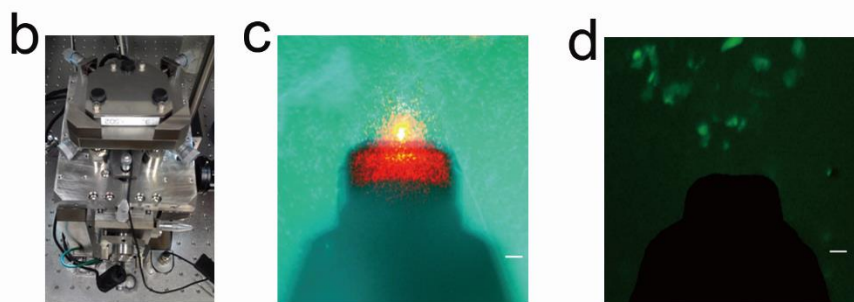
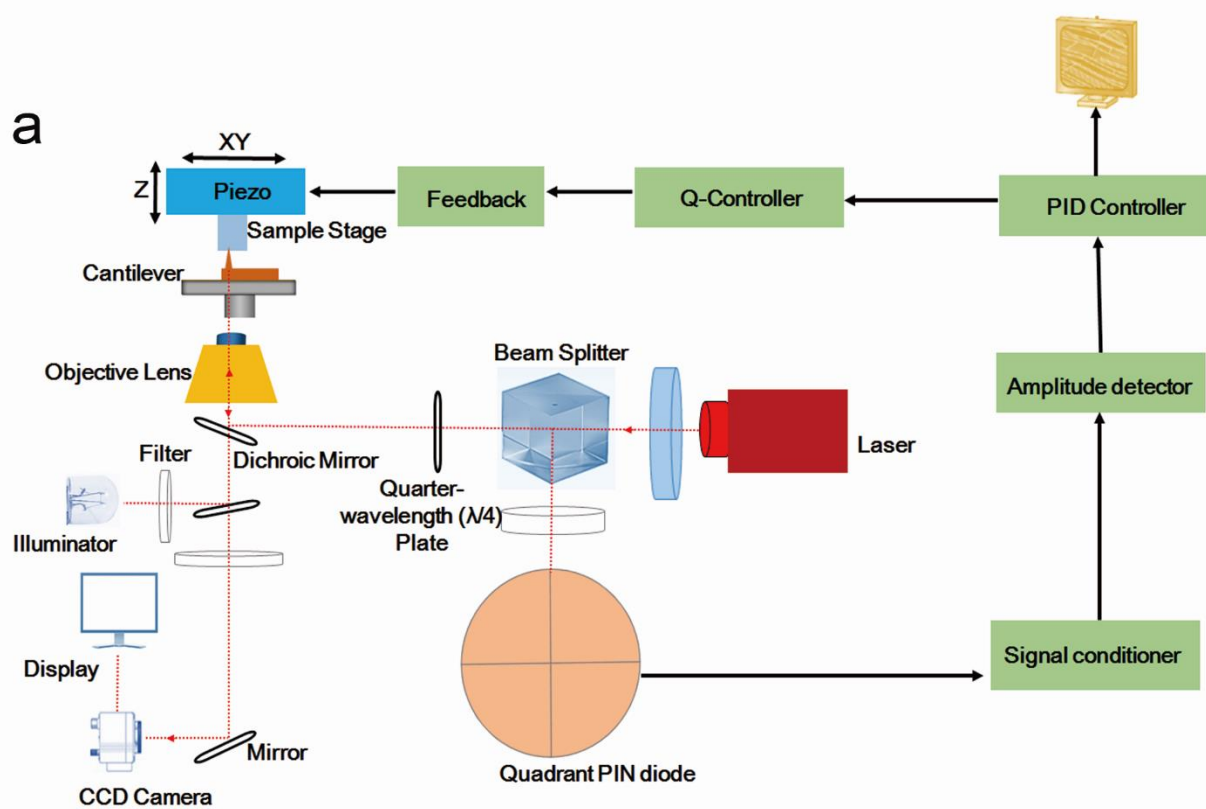
[‡] Bio-AFM Frontier Research Center, Kanazawa University, Kakuma-machi, Kanazawa 920-1192, Japan;

[§]Division of Natural System, School of Natural Science and Technology, Kanazawa University, Kakuma-machi, Kanazawa, Japan

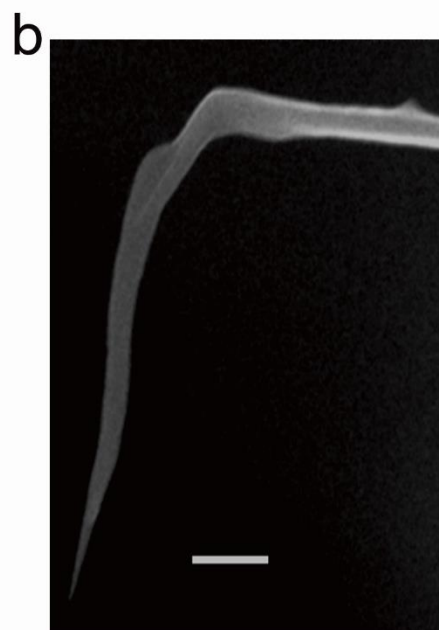
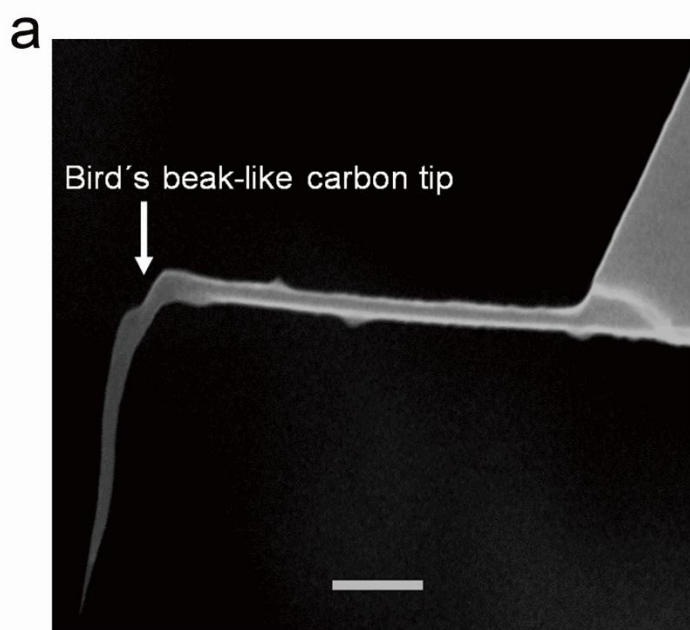
^{//} Division of Translational and Clinical Oncology, Cancer Research Institute, Kanazawa University, Kanazawa, Japan.

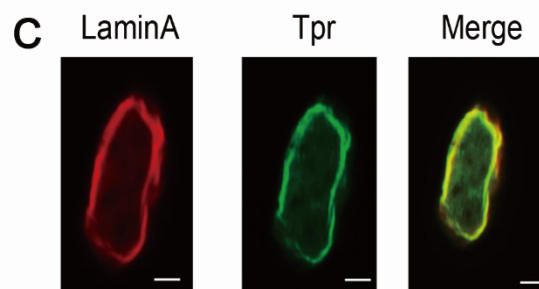
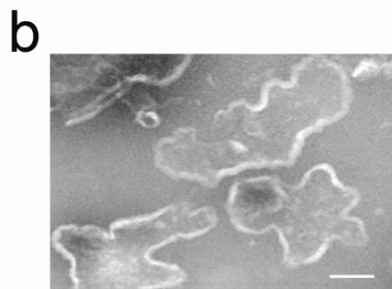
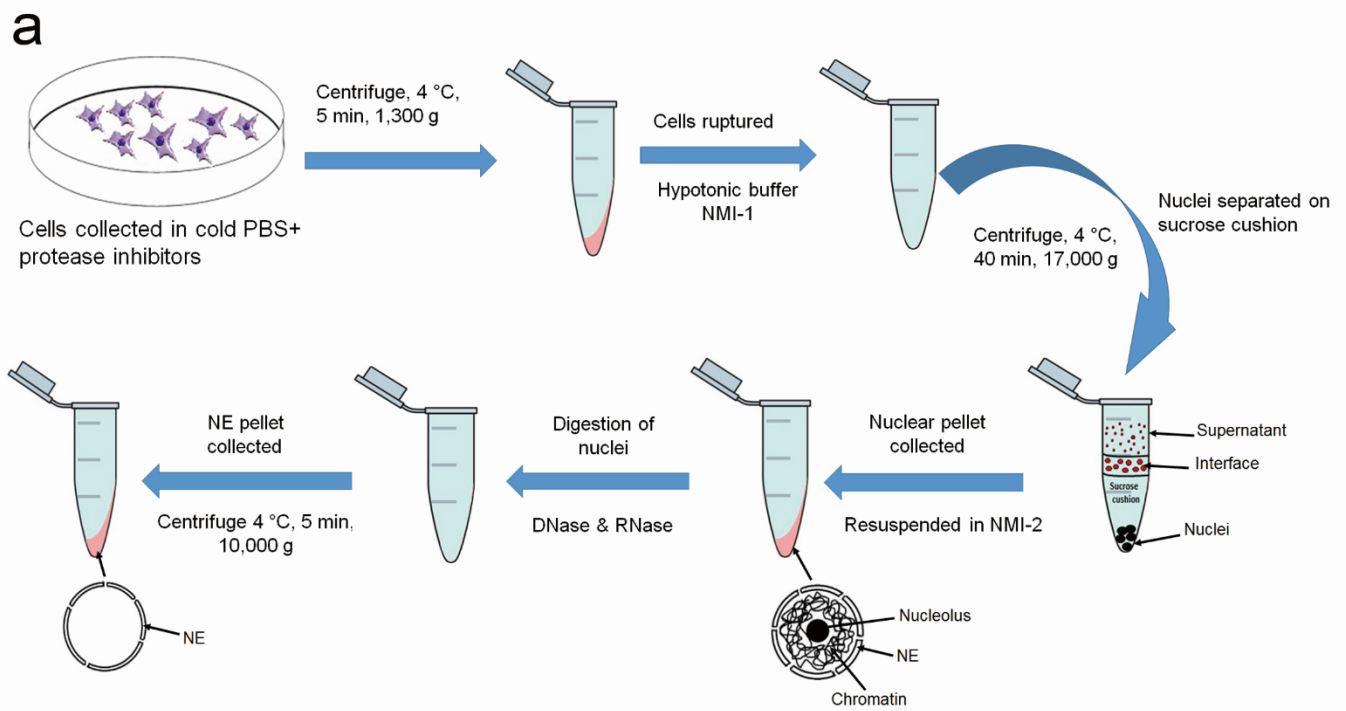
Supporting Information

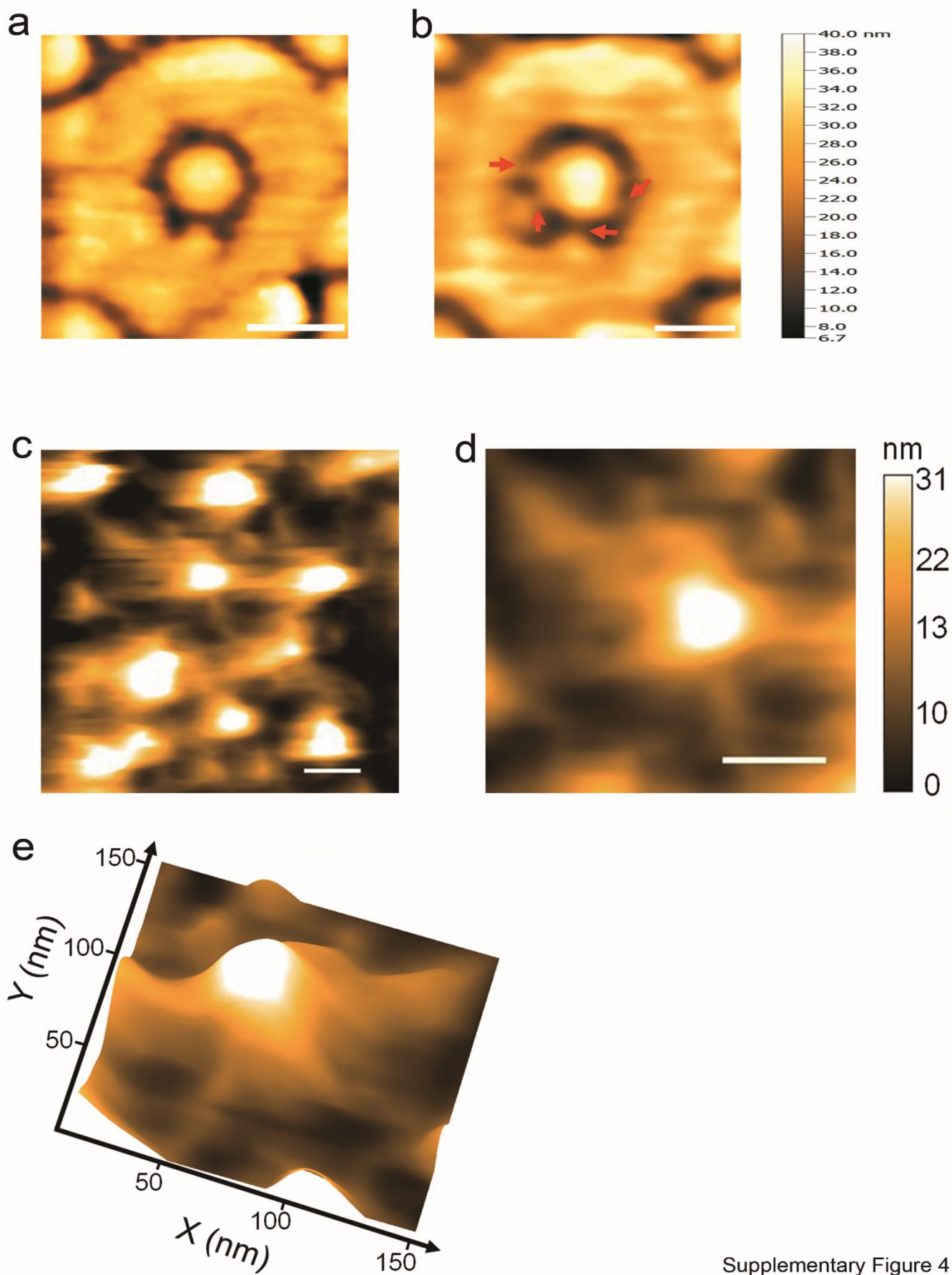
- **Supplementary Figure (Fig. S1-S8)**
- **Supplementary Figure legend (Fig. S1-S8)**
- **Supplementary Table 1.**
- **Movie captions (Movie 1-11)**
- **Supplementary Method**



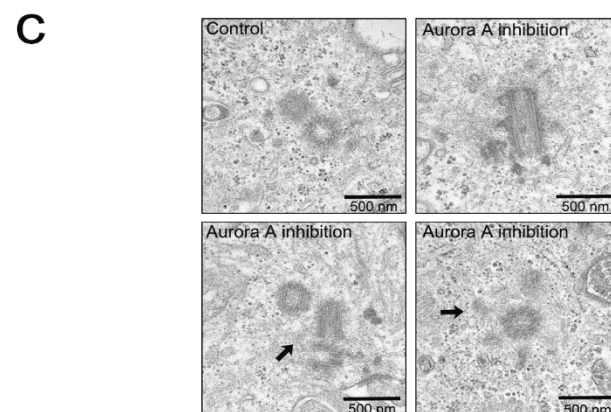
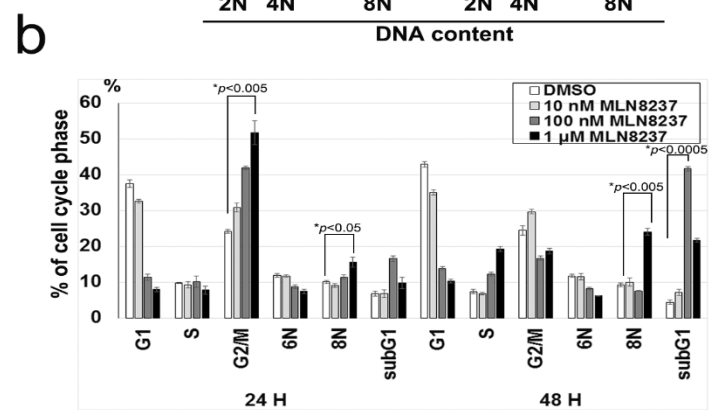
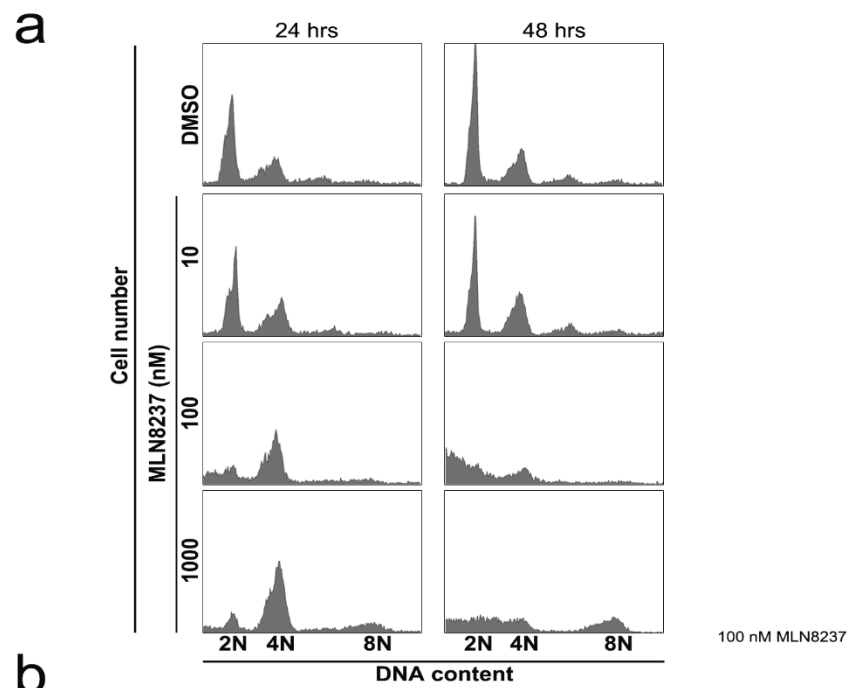
Supplementary Figure 1

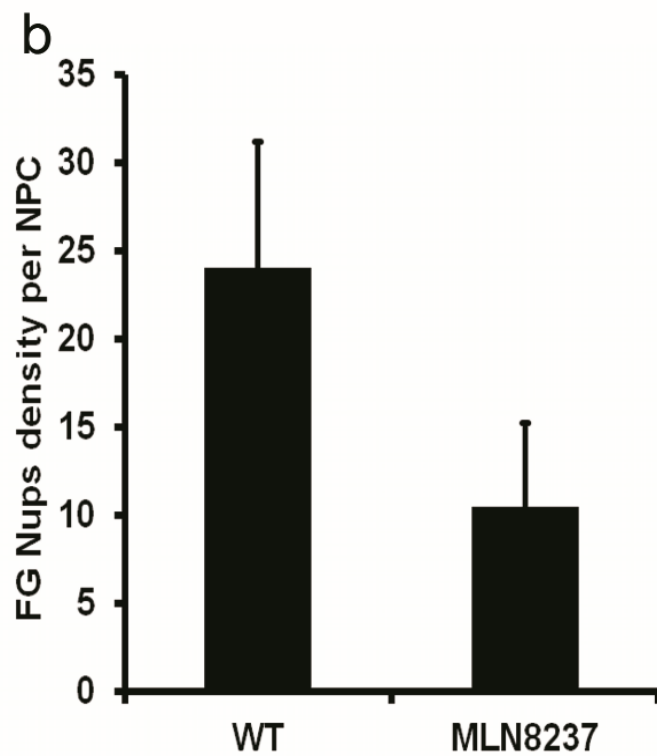
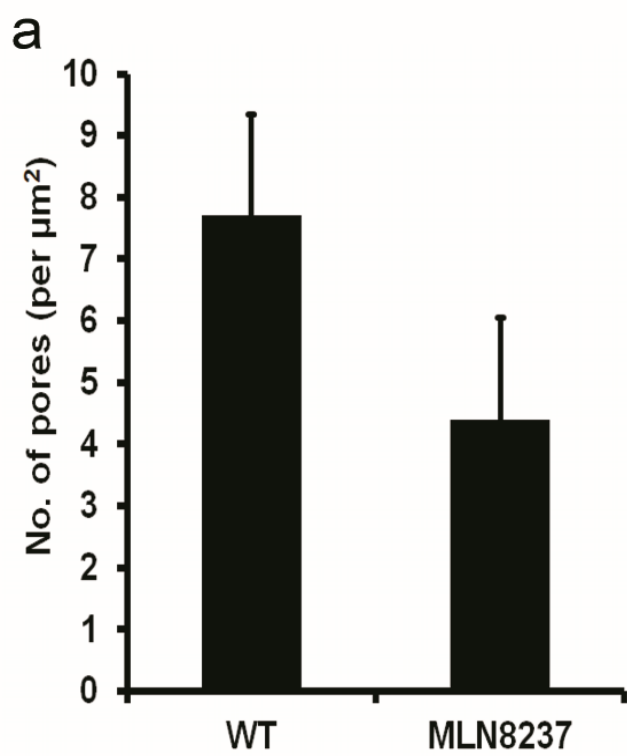






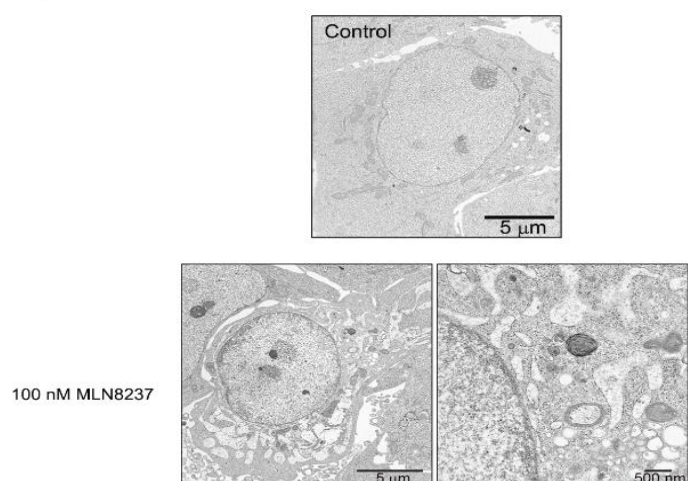
Supplementary Figure 4



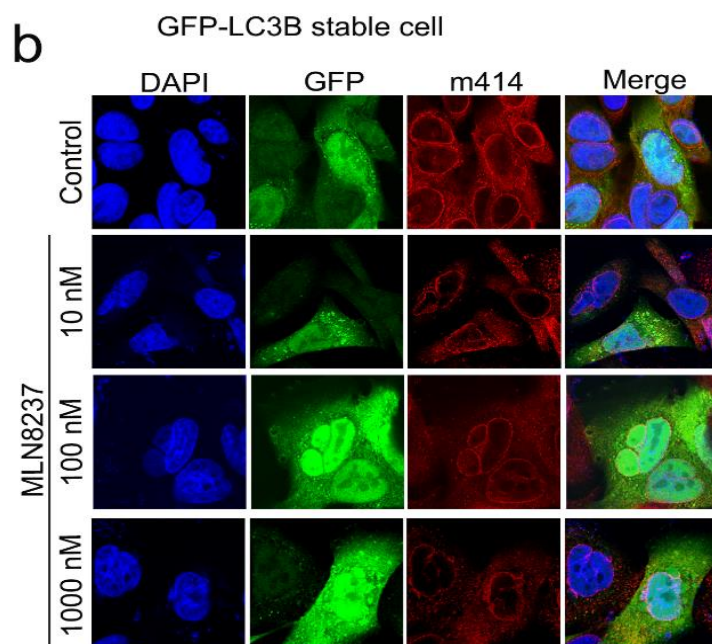


Supplementary Figure 6

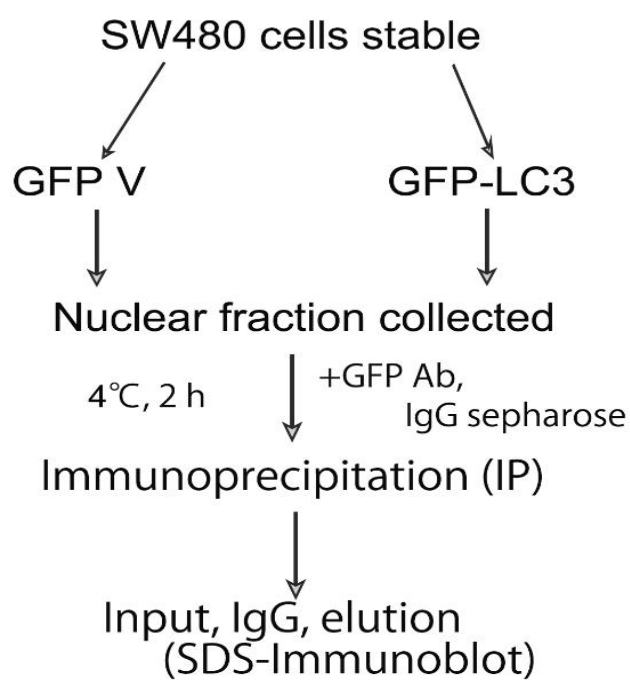
a



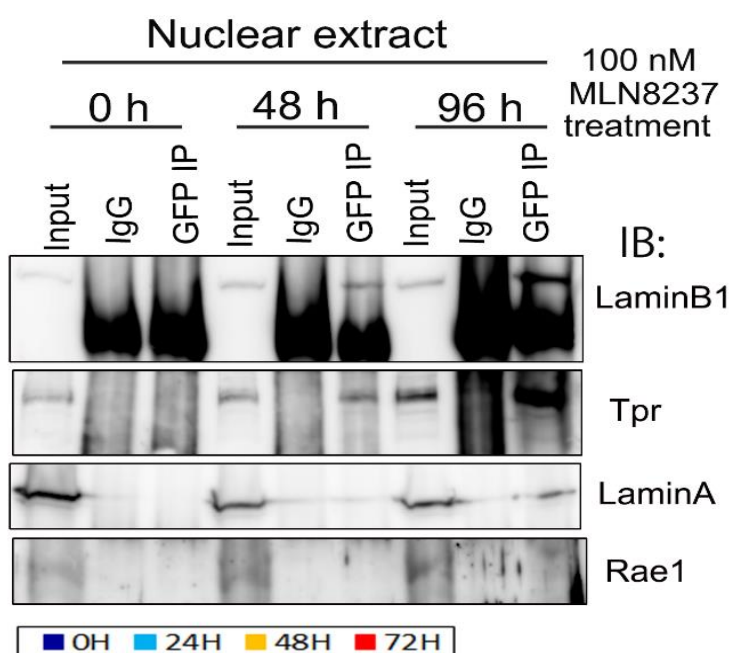
b



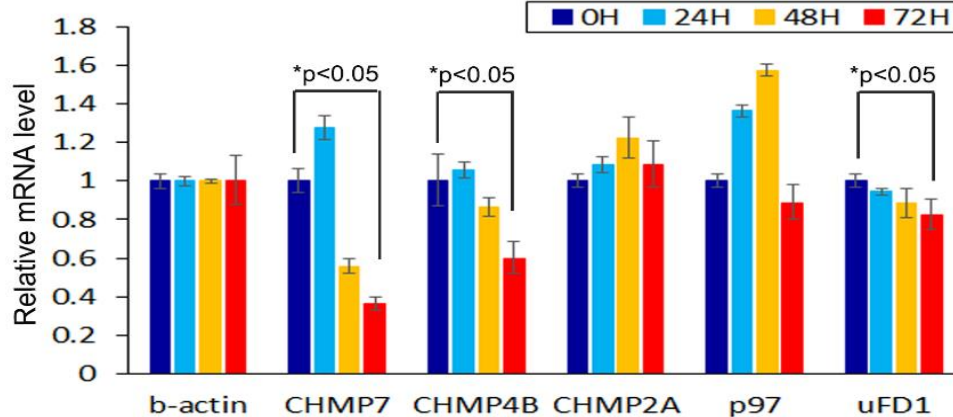
c



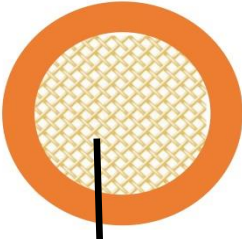
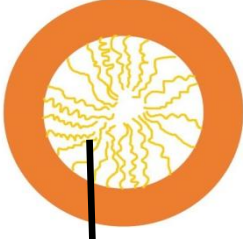



d



e



Supplementary Figure 7

Model	Hydrogel	Virtual gating/ Polymer brush	Forest	Reduction of dimensionality	Cobweb
References	Frey S et al., 2006. Frey S & Gorlich DA, 2007. Frey S & Gorlich DA, 2009. And others.	Rout MP et al., 2000. Rout MP et al., 2003. Lim RY et al., 2007. Sakiyama Y. et al., 2016. And others.	Patel SS et al., 2007. And others.	Peters R, 2005. And others.	Current study.
Diagram	 <p>Sieve-like meshwork</p>	 <p>Polymer brush</p>	 <p>Area 1 Area 2</p>	 <p>FG domain coat</p>	 <p>Cobweb FG network</p>

Supplementary Figure 8

	Gene name		Primer
ESCRTIII	CHMP7	F	gtctctcaaggccaagcaac
	CHMP7	R	tgtctgggaggcatagatcc
	CHMP4B	F	cgaaacctgtagggttga
	CHMP4B	R	ctgttcgggtccactgatt
	CHMP2A	F	caggctgtgtccctcaagat
	CHMP2A	R	ggcaacttcagctgtctgt
	p97	F	gagctcctcaatgtgggtgt
	p97	R	ccaatcgagacatagctga
	uFD1	F	gaacccgaaagacaagtcca
	uFD1	R	cccccttctctttccatcc
FG-Nups	Nup358	F	aaacgaggtcaatggcaaac
	Nup358	R	gagaggcttcaggttcacg
	Nup214	F	cattcagcctgctgttgca
	Nup214	R	agacagaaaggctgatcg
	Nup153	F	gcagctctgcctttggaac
	Nup153	R	aagacaaatggggtgacagc
	Nup98/96	F	actgggacagcatttggaac
	Nup98/96	R	aaacagggtcgaaccaacag
	Rae1	F	gctgctgggaagtcaagac
	Rae1	R	tcgtcactccagcagacatc
House keeping	beta-actin	F	tgacaggatcgagaaggaga
	beta-actin	R	cgctcaggaggagcaatg

Supplementary Figure legends

Supplementary Figure 1. Fluorescent HS-AFM. (a) The HS-AFM system combined with a fluorescent CCD camera. (b) HS-AFM stage with a z-piezo scanner. (c) Bright field of the CCD camera showing HCT116 NEs, scale bar, 5 μm . (d) CCD camera display showing GFP-tagged NEs on the glass stage approached by a cantilever tip; scale bar, 5 μm .

Supplementary Figure 2. Cantilever preparation. Carbon tip grown on the cantilever body by EBD using Scanning Electron Microscope (SEM). (a) Side view of a cantilever body; scale bar, 1 μm . (b) Side view of a cantilever sharpened tip with a length and radius of approximately 2 μm and 8 nm, respectively; scale bar, 500 nm.

Supplementary Figure 3. Nuclear envelope purification. (a) Sucrose cushion method to isolate the NEs of HCT116 cells. (b) EM micrograph showing purified NEs; scale bar, 500 nm. (c) Confocal microscopy micrograph showing immune-stained NEs with anti-LaminA and anti-Tpr antibodies; scale bar, 5 μm .

Supplementary Figure 4. HS-AFM observation of plugged-NPCs and nuclear basket.

- (a) HS-AFM image of an NPC with a central plug inside the central channel. Z-scale=40 nm, speed is 2 frames per second with 200×200 pixels, scale bar, 50 nm.
- (b) HS-AFM image showing the FG-Nup filaments interacting with the existing central plug (Red arrows). Z-scale=40 nm, speed is 2 frames per second with 200×200 pixels, scale bar, 50 nm.
- (c) Nuclear baskets extend beyond from the inner nuclear membrane. Z-scale=31 nm, speed=2 frame/s with 200×200 pixels; scale bar, 100 nm.
- (d) Average structure of a nuclear basket displaying distinct nuclear filaments that fuse into a basket distal ring (scale bar; 100 nm).
- (e) 3D view of a single representative nuclear basket in (b)

Supplementary Figure 5. Effect of MLN8237 on cell cycle progression.

- (a) HCT116 cells were treated with MLN8237 for 24 or 48 h, and cell-cycle progression was analysed by flow cytometry.
- (b) The percentages of G1, G2/M, S, and sub-G1 cells were calculated based on the results shown in (a). Asterisks indicate significant *p*-values (**p* < 0.05 or ***p* < 0.005).
- (c) Electron microscopic images of control or MLN8237-treated HCT116 mitotic cells. Black arrow indicates abnormal configuration of centrosomes Scale bars, 500 nm.

Supplementary Figure 6. Distribution of NPCs and FG-Nups.

(a) The distribution of NPCs on the NE surface of WT and MLN8237-treated cells. The graph showing the number of pores per μm^2 .

(b) The density of FG-Nup filaments in WT and MLN8237-treated NPCs. The graph showing the number of single FG-Nup filaments observed by HS-FM in a single NPC central channel, N=10.

Supplementary Figure 7. Oncogene-induced senescence (OIS) enhanced cytoplasmic LC3 nuclear influx interacting with Tpr and Lamin B1 facilitated by NE and NPC rupture in dying CRC cells.

(a) Electron microscopic images of control or MLN8237-treated HCT116 cells. Insets are magnifications of the vacuole regions in the observed cells.

(b) Representative confocal images of MLN8237-treated GFP-LC3 stable SW480 cells, stained with GFP (green) and mAb414 (red) at the indicated concentrations. Goat anti-mouse Alexa Fluor-488 or rabbit rhodamine were used as secondary antibodies. DNA was counterstained using DAPI.

(c) Schematic of the experimental work flow for the identification of proteins interacting

with LC3 in the nucleus.

(d) Nuclear extracts containing GFP or GFP-LC3 were incubated with anti-GFP antibody-sepharose resin for 2 h at 4 °C to immunoprecipitate GFP or GFP-LC3 protein complexes (IP). IP fractions were washed three times and then eluted from the beads. The input, IgG, and eluted IP fractions were then analysed by immunoblotting. IP fractions from nuclear SW480 extracts were resolved by SDS-PAGE and immunoblotted with the indicated antibodies.

(e) HCT116 cells were treated with DMSO (control) or MLN8237 for 0, 24, 48, or 72 h, and the mRNA levels of ESCRT III factors were subsequently assayed by quantitative PCR. The data are presented as the means \pm S.D. for triplicate determinations. Bars, S.D.

* $p < 0.05$.

Supplementary Figure 8. A schematic illustration of various Nucleocytoplasmic transport models.

This figure illustrates in a simple diagram-pattern the main differences between the previously proposed models and the current studied model. In the hydrogel model, FG-repeats form a homogenous sieve-like meshwork inside the central channel. In the virtual gating/polymer brush model, FG-Nups extend inside the central channel as repulsive

bristles or polymer brushes composing an entropic barrier. In the forest model, a two-gate model of NPC is proposed, in which a central diffusion gate composed of cohesive FG-Nup filaments (Area 1) and a peripheral gate composed by repulsive FG-Nup filaments (Area 2). In the reduction of dimensionality model, FG domains continuously form an inner coat (Red inner layer) on the inner wall of the NPC to provide a continuous sites for NTRs and cargos.⁴⁵

Supplementary Table 1.

Sequences of PCR primers used in this study.

Movie captions

Movie 1a: A $300 \times 300 \text{ nm}^2$ area of the cytoplasmic face of a HCT116 cell NE with many native NPCs. Z-scale=6 nm, speed=5 frames/s) with 200×200 pixels. This movie is played back in real time. Scale bar, 100 nm.

Movie 1b: This movie shows a single representative NPC. It is cropped from the original captured movie in Supplementary Movie 1a from a $120 \times 120 \text{ nm}^2$ area (Z-scale=6 nm, speed=5 frames/s) with 200×200 pixels. Scale bar, 50 nm.

Movie 1c: This movie shows a $120 \times 120 \text{ nm}^2$ area of a single NPC with successive dynamic changes. (Z-scale=6 nm, speed=5 frames/s) with 200×200 pixels. Scale bar, 50 nm.

Movie 1d: This movie shows the native WT central channel dynamic changes over the elapsed time. It is played back in real time but is shown in greys to clearly illustrate the flexibility. This movie is cropped from the original captured movie in Supplementary Movie 1a from $120 \times 120 \text{ nm}^2$ (Z-scale=6 nm, speed=5 frames/s) with 200×200 pixels. Scale bar, 20 nm.

Movie 2: This movie shows a $250 \times 320 \text{ nm}^2$ area of the nuclear basket of a HCT116 cell NE with many pre-fixed NPCs. Z-scale=31 nm, speed=2 frame/s with 200×200 pixels; scale bar, 100 nm.

Movie 3a: Typical mitotic cell death of an SW480 cell expressing GFP-Lamin B1 after being treated with MLN8237 for 1 h. (Phase contrast mode) Time interval: 24 h.

Movie 3b: Typical mitotic cell death of an SW480 cell expressing GFP-Lamin B1 after being treated with MLN8237 for 1 h. (GFP mode) Time interval: 24 h.

Movie 4a: Bi-nuclei and bi-cell fusion in a dying SW480 cell expressing GFP-Tpr, 24 h after MLN8237 treatment. (Phase contrast mode) Time interval: 24 h.

Movie 4b: ‘Nuclear-fusion’ phenotype (partial loss of NE and NPC) in a dying SW480 cell expressing GFP-Tpr, 48 h after MLN8237 treatment. (Phase contrast mode) Time interval: 4 h.

Movie 4c: ‘Nuclear-fusion’ phenotype (partially loss of NE and NPC) in dying SW480 cell expressing GFP-Tpr, 48 h after MLN8237 treatment. (GFP mode) Time interval: 4 h.

Movie 4d: Another example of reversible nuclear budding in a dying SW480 CRC expressing GFP-Tpr (FG-Nup), 48 h after MLN8237 treatment. (Phase contrast mode) Time interval: 24 h.

Movie 4e: Typical nuclear rupture induced an influx in a dying HCT116 cell expressing GFP-Nup358, 48 h after MLN8237 treatment. (GFP mode) Time interval: 24 h.

Movie 5a: A typical dying SW480 cell expressing GFP-Tpr, 12 h after MLN8237 treatment. (GFP mode) Time interval: 24 h.

Movie 5b: An SW480 cell expressing GFP-LC3 in DMSO. (GFP mode) Time interval: 4 h.

Movie 5c: An SW480 cell expressing GFP-LC3, 12 h after MLN8237 treatment. (GFP mode) Time interval: 4 h.

Movie 5d: ‘Nuclear-explosion’ phenotype in an SW480 cell expressing GFP-LC3, 48 h after MLN8237 treatment. (Phase contrast mode) Time interval: 4 h.

Movie 5e: Nucleophagy in a dying SW480 cell expressing GFP-Tpr (FG-Nup), 48 h after MLN8237 treatment. (GFP mode) Time interval: 24 h.

Movie 6a: Dying NPCs after MLN8237 treatment (100 nM, 48 h). This is a $300 \times 300 \text{ nm}^2$ area of the NE cytoplasmic face with many native NPCs. This movie was recorded at 300 ms/frame (Z-scale=20 nm, speed=3.3 frames/s) with 200×200 pixels. This movie is played back in real time. Scale bar, 100 nm.

Movie 6b: A $120 \times 120 \text{ nm}^2$ area in an individual dying NPC after MLN8237 treatment (100 nM, 48 h). This movie was cropped from the original captured movie in Supplementary Movie 6a from a $120 \times 120 \text{ nm}^2$ area (Z-scale=20 nm, speed=3.3 frames/s) with 200×200 pixels. Scale bar, 50 nm.

Movie 7a: The left panel of this movie shows the original FG-Nups inside the central

channel of a WT NPC, and the right panel shows the same FG-Nups after using a FFT bandpass filter (using ImageJ to reduce the noise and show the tiny FG filaments inside the central channel). Disordered and entangled FG threads can be observed in this movie. Speed=6.7 frames/s; scale bar, 50 nm.

Movie 7b: The left panel of this movie shows the original FG-Nups inside the central channel of an MLN8237-treated NPC, and the right panel shows the same FG-Nups after using a FFT bandpass filter (using ImageJ to reduce the noise and show the tiny FG filaments inside the central channel). Traces of the FG network can be observed in some frames in this movie. Speed=3.3 frames/s; scale bar, 50 nm.

Movie 8a: This movie is a magnification of the WT central channel visualized in **Movie 7a**.

Movie 8b: This movie is a magnification of the MLN8237-treated central channel visualized in **Movie 7b**.

Movie 9a: The native FG-Nups web inside the central channel of the WT NPC is resolved in this movie by using high speed imaging (Z-scale=19 nm, speed=6.7 frames/s). A 40×40

nm² area with 200×200 pixels. The frames show the FG network in an extra rapid motion with entangled FG threads retracting and elongating in a cobweb-like network. Scale bar, 10 nm.

Movie 9b: Traces of the FG web inside the central channel of an MLN8237-treated NPC (Z-scale=19 nm, speed=3.3 frames/s). The frames show that the FG network has almost lost its architecture and shows elongated filaments through the channel. Scale bar, 10 nm.

Movie 10a: A slow motion play back of **Movie 9a** to show the dynamics of the FG-Nups web of a WT NPC. Speed=2 frames/s.

Movie 10b: A slow motion play back of **Movie 9b** to show the degraded FG-Nups web of the dying NPC. Speed=2 frames/s.

Movie 11. HS-AFM observation of an NPC with a central plug. This movie is showing a native nuclear pore complex with a central plug in the central channel showing a dynamic motion. Z-scale=40 nm, speed is 2 frames per second with 200×200 pixels, scale bar, 50 nm.

Supplementary Methods

HS-AFM

To image fragile biological samples using HS-AFM, the oscillating cantilever tip has to tap the sample surface with a small force. To do so, the amplitude set point, A_s of a force-feedback controller has to be set very close to the free oscillation peak-to-peak amplitude, A_0 . This condition however promotes tip-parachuting and increases its duration, making horizontal lines in AFM images. To avoid this, the current HS-AFM has an advanced PID controller (named a dynamic PID controller) with a capability to automatically change the PID's gain parameters, depending on the cantilever oscillation amplitude.^{1,2} When the amplitude exceeds a threshold level (set at the amplitude set point or slightly above), the gains are increased. The oscillation amplitude thereby quickly returns towards the set point before the error signal is saturated. Consequently, the feedback bandwidth becomes independent of the set point as long as the set point is smaller than 0.9–0.95. When a piezoactuator is driven continuously for a long time, its temperature is increased. As a result, the extension coefficient of the piezoactuator is usually lowered to some extent. In the tapping mode, a cantilever is continuously excited by a sinusoidally oscillated piezoactuator placed at the cantilever holder. The cantilever free oscillation amplitude A_0 gradually declines by the thermal effect. When A_0 is set at 3 - 4 nm and the set point A_s is set at $0.9 \times A_0$ (these values are routinely used for imaging delicate biological samples),

their difference ($A_0 - A_s$) is only 0.3 – 0.4 nm. Under this condition, the downward drift of A_0 easily leads to complete dissociation of the cantilever tip from the sample surface because the feedback system misinterprets the change in the cantilever oscillation amplitude and hence withdraws the sample stage from the cantilever tip. Thus, to achieve stable imaging under a small tapping force, A_0 has to be kept constant precisely.

Estimation of tapping force applied to the sample surface

Average tapping force, $\langle F \rangle$ applied to the sample surface is expressed as

$$\langle F \rangle = \frac{k_c A_0}{2Q_c} \sqrt{1 - r^2}$$

where k_c is the cantilever spring constant, Q_c is the quality factor of the cantilever resonance, A_0 is the cantilever's free oscillation peak-to-peak amplitude, r represents the ratio of the amplitude set point, A_s of a force-feedback controller to A_0 (i.e., $r = A_s/A_0$, $0 < r < 1$). Using a typical imaging condition used in the present study (i.e., $k_c = 0.2$ N/m, $Q_c = 2$ for the HS-AFM cantilevers (BL-AC7DS-KU2, Olympus), $A_0 = 3 - 4$ nm, $r = 0.9$), $\langle F \rangle$ can be estimated to be 65 – 90 pN. In addition, we estimated F_{max} to be 70 – 80 pN in all NPC experiments. However, in HS-AFM the impulse (= Force \times time) is a more meaningful mechanical quantity because this describes the momentum transfer in the short time it takes the tip to make a single tap, which in the present study is less than 0.1 μ s. Thus, as demonstrated in many studies by HS-AFM,³ the expected effect on the NPC

is very small which ensure that any disruption to the FG Nups is almost reduced.

Image alignment

The HS-AFM movies were processed to remove thermal drift in x, y and z-directions and to reduce the high frequency noise in x, y direction (z-scanner noise) by Image J software.

First, the horizontal noise was reduced by the median filter with 2.0-radius. Second, the z-directional drift was removed by background subtraction of each frame with the primary functions in x- and y-directions, which resulted in no difference in average height between frames. At last, the horizontal drift was removed by using the template-match algorithm, where each frame was translated in xy-plane to maximize a normalized cross correlation coefficient between the frame being translated and the reference frame.

Supporting Information References:

- (1) Koder, N.; Sakashita, M.; Ando, T. Dynamic Proportional-Differential Controller for High-Speed Atomic Force Microscopy. *Rev. Sci. Instrum.* 2006, *77*, 083704.
- (2) Ando, T. High-Speed Atomic Force Microscopy. *Microscopy (Oxf)* 2013, *62*, 81–93.
- (3) Ando, T.; Uchihashi, T.; Scheuring, S. Filming Biomolecular Processes by High-Speed Atomic Force Microscopy. *Chem Rev.* 2014, *114*, 3120–3188.